Published in final edited form as:
ACS Appl Mater Interfaces. 2009 July ; 1(7): 1474–1481. doi:10.1021/am9001293.

Near infrared phosphorescent polymeric nanomicelles: efficient optical probes for tumor imaging and detection

Rajiv Kumar[1], **Tymish Y. Ohulchanskyy**[1], **Indrajit Roy**[1], **Sandesh K. Gupta**[1], **Carsten Borek**[2], **Mark E. Thompson**[2], and **Paras N. Prasad**[1,*]

[1]Institute for Lasers, Photonics and Biophotonics, SUNY at Buffalo, Buffalo NY 14226

[2]Department of Chemistry, University of Southern California, Los Angeles, CA 90089

Abstract

We report a formulation of near infrared (NIR) phosphorescent polymeric nanomicelles and their use for in vivo high contrast optical imaging, targeting and detection of tumors in small animals. NIR phosphorescent molecules of Pt(II)-tetraphenyltetranaphthoporphyrin [Pt(TPNP)] were found to maintain their NIR phosphorescence properties when encapsulated into phospholipid nanomicelles. The prepared phosphorescent micelles are of ~100 nm size and are highly stable in aqueous suspensions. A large spectral separation between Pt(TPNP) absorption, peaked at ~700 nm, and its phosphorescence emission, with peak at ~ 900 nm, allows a dramatic decrease in the level of background autofluorescence and scattered excitation light in the NIR spectral range, where the signal from phosphorescent probe is observed. *In vivo* animal imaging with subcutaneously xenograted tumor-bearing mice has resulted in high contrast optical images, indicating highly specific accumulation of the phosphorescent micelles into tumors. Using optical imaging with NIR phosphorescent nanomicelles, detection of smaller, visually undetectable tumors has also been demonstrated.

Keywords

Optical imaging; Near Infra Red (NIR); Phosphorescence; nanomicelles

INTRODUCTION

In the arena of bioimaging, optical imaging possesses a unique position, providing the highest sensitivity and spatial resolution. Optical imaging with fluorescent probes is the only technique which provides cellular or molecular level information with almost single molecule sensitivity. Therefore, it is being widely used for tracking and reporting functional information on molecules, proteins, and cells/tissues *in vitro* and in *vivo*, with a wide range of applications including early diagnosis of cancer and other diseases, study of pharmacokinetics and pharmacodynamics of biomolecules *in vivo*, and gene expression in light-producing transgenic animals.[1, 2] However, *in vivo* applications of optical bioimaging are severely limited owing to the poor tissue penetration of visible light. Therefore, in recent years there is a surge in the development of new generation of optical probes, which absorb and emit light in the near infra-red (NIR) range (~700-1000 nm). This spectral region is considered as the “optical transmission window” of biological tissues where there is less

* To whom correspondence should be addressed: pnprasad@buffalo.edu.

SUPPORTING INFORMATION AVAILABLE: Details of transmission electron microscopy, *in vivo* optical imaging setup, MTS assay, release kinetics studies, PL quantum yield measurements and PL images. This material is available free of charge via the Internet at http://pubs.acs.org.

absorption and scattering of the excitation and emitted light as well as reduced autofluorescence, thus allowing penetration of light for deep-tissue imaging with higher contrast.[2-4] Recent rise in nanotechnology has further bolstered the prospects of *in vivo* optical imaging through the development of a variety of NIR-luminescent nanoformulations, which include quantum dots,[5] upconverting nanophosphors,[6] and luminophore-containing nanoparticulate carriers such as liposomes,[7] polymersomes,[8] ceramic,[9-11] or polymeric[12] nanoparticles, etc.

Despite a large amount of efforts currently being directed to fight cancer, it continues to be one of the principal diseases, which leads to a large number of fatalities in the world. This is primarily because using currently available techniques the clinical diagnosis of cancer is possible only at extremely advanced phases, when the tumor has extensively metastasized over the body and is thus beyond surgical or chemo-radiative intervention. As per the statistical NIH database on the pancreatic cancer, currently available on the NIH website, 53% of the pancreatic cancer patients have been diagnosed after the cancer has already been metastasized (distant stage). Therefore, there is an urgency in the development of novel imaging probes which will diagnose the disease at an earlier, pre-metastatic phase, thus significantly reversing the poor prognostic scenario associated with this disease. NIR-luminescent nanoparticles are fast emerging as extremely promising candidates in this direction, as new generation of optical probes for *in vivo* imaging. Nanoparticulate optical probes doped with organic NIR fluorescent molecules demonstrate a number of advantages over molecular NIR fluorescent probes. Firstly, the nanoparticle formulations provide an option for multimodal imaging by co-doping with imaging agents of other modality, such as MRI[12, 13] or PET/SPECT[14, 15] imaging, thus allowing to obtain complementary anatomical and physiological information. Next, the surface of nanoparticles can be easily modified with (a) inert and biocompatible polymers such as polyethyleneglycol (PEG), which endow them with the ability to evade capture and degradation by the reticuloendothelial system (RES)[16, 17], as well as (b) biorecognition molecules to target specific tissues *in vivo* ("active targeting").[18-21] Finally, upon systemic administration, nanoparticles have inherent property to be preferentially taken up by the malignant tissues ("passive targeting") by virtue of the "enhanced permeability and retention" (EPR) effect[22, 23], which is the property of such tissues to engulf and retain circulating macromolecules and particles owing to their "leaky" vasculature and poor lymphatic drainage.

Polymeric nanomicelles (PNMs) made up of biocompatible, hydrophobic-hydrophilic copolymers (e.g. poloxamers, ploxamines, pluronics, etc.), encapsulating a variety of diagnostic and therapeutic agents, are being increasingly investigated pre-clinically as safe and efficient drug delivery systems.[24] The biocompatible composition of the PNMs, as well as their small size and tunable surface properties, enable them to avoid capture/degradation by RES, thus allowing their unimpeded, prolonged systemic circulation. Drugs encapsulated within PNMs are reported to exhibit higher passive accumulation in tumors compared to free drugs with reduced distribution in other tissues. Recently, PNMs based upon diacyllipid-poly(ethylene glycol) composite molecules have attracted significant attention in drug delivery due to their many unique characteristics. These micelles are stable at extremely low concentrations and demonstrate an increased EPR-mediated passive tumor accumulation.[22] In addition, these micelles can be actively targeted to tumor and other desired sites via conjugation with targeting ligands.[25, 26]

In this communication, we report the use of polymeric nanomicelles encapsulating NIR phosphorescent dye [Pt(II)-tetraphenyltetranaphthoporphyrin, Pt(TPNP)] as efficient probes for the high contrast optical imaging and diagnosis of tumors in small animals. Such phosphorescent molecules as heavy-metal-ligand complexes have been extensively used in the development of the organic light emitting devices (OLED).[27-35] Compared with organic

fluorescent dyes, they possess interesting photophysical properties, which make them attractive candidates as probes for autofluorescence-free optical bioimaging. The crucial advantage of the NIR phosphorescent optical probes over conventional NIR-fluorescent probes is a large spectral separation between absorption and phosphorescence emission which ensures a dramatic decrease in the level of background autofluorescence and scattered excitation light in the spectral range where the signal from phosphorescent probe is observed. In addition, the phosphorescence lifetime for these molecules is essentially different from the characteristic fluorescence lifetime, allowing an opportunity to exploit this highly characteristic feature for time-resolved photoluminescence (PL) imaging.[36-40] Time-gated detection can dramatically increase the contrast in imaging, allowing reconstruction of the phosphorescence intensity and lifetime images in scattering (or autofluorescent) volumes.[39, 40] A few reports have been recently published on the use of phosphorescent molecules emitting in the visible range for optical imaging *in vitro*,[36-38, 41-45] as well as biolabeling[44] and flow cytometry[45]. Formulations of polymeric nanoparticles encapsulating molecules, which phosphoresce in the visible range, have been also reported. However, they are phosphorescent at room temperature only if the atmospheric oxygen is removed,[46] or in special polymeric matrix impermeable to oxygen[47-49] or, additionally, when the nanoparticle matrix consists of halogen-containing copolymers,[49] which are potentially harmful for *in vivo* applications. On the other hand, in vivo imaging with phosphorescent probes has been known for a long time. Wilson and co-authors first proposed the use of the phosphorescent metalloporphyrins as the oxygen-sensitive probes for imaging hypoxic tissues in vitro and vivo.[50, 51] Wilson, Vinogradov and co-authors have further developed their approach, allowing use of phosphorescent probes as oxygen sensors and imaging probes for in vitro and in vivo applications involving imaging of the hypoxic cells and tissues.[52] However, these applications were not aimed at the specific targeting of tumors with phosphorescent imaging probes, as tumor sites were not the only sites that were shown to be hypoxic. Here we report the application of a promising and efficient formulation of NIR phosphorescent polymeric nanomicelles for high contrast optical imaging *in vivo*, allowing targeting and detection of tumors in live animals.

EXPERIMENTAL

Pt(II)-tetraphenyltetranaphthoporphyrin [Pt(TPNP)] was prepared by literature procedures.[35, 53] The encapsulation of the Pt(TPNP) into the DSPE-PEG/PC phospholipid micelles was carried out as reported earlier[54, 55] and shown in Figure 1 with several modifications. Typically, 100μL of phosphorescent dye stock solution in toluene (0.12mg/ml) was evaporated and dried under vacuum. The obtained solid mass was then resuspended in 1mL chloroform with 5.5×10^{-6} moles of phospholipids containing 20% of 1,2-distearoyl-*sn*-glycero-3-phosphoethanolamine-N-[methoxy(polyethylene glycol)-2000] (DSPE-mPEG-2000), 20% of 1,2-distearoyl-*sn*-glycero-3-phosphoethanolamine-N-[amino(polyethylene glycol)-2000] (DSPE-PEG-2000 NH_2) and 60% of 1,2-distearoylglycero- 3-phosphocholine (DSPC), all from Avanti Polar Lipids, Inc., Alabaster, AL. The solution was sonicated for 1 min and evaporated the chloroform completely under vacuum over the rotary evaporator, following which the residue was gently heated at 80 °C and 2 mL of water was added to obtain an optically clear suspension containing DSPE-PEG/PC micelles. Dye/micelle formulation was purified by ultracentrifugation at 500,000 g for 2 hrs. The supernatant was discarded and the pellet containing phosphorescent dye-micelles was resuspended in water. Different concentrations of the dye loaded nanomicelles were prepared in the same way as described above by varying the polymer to dye ratio. All the formulations of the phosphorescent dye with approximate concentrations of 2.5, 12.5, 25 μM were stable in deionized water or phosphate buffered saline (PBS), with no observable aggregation, dissociation or bleaching for at least 1 month of storage. The samples were stored at 4 °C for further use.

Absorption spectra were acquired using a Shimadzu 3600 spectrophotometer and a SPEX 270M spectrometer (Jobin Yvon), equipped with InGaAs TE-cooled photodiode (Electro-Optical Systems, Inc.), was used to record emission spectra. A laser diode emitting at 630 nm was used as an excitation source. The sample in a quartz cuvette was placed directly in front of the entrance slit of the spectrometer and the emission signal was collected at 90-degrees relative to the excitation light. A Hamamatsu IR-PMT, attached to second output port of the SPEX 270M spectrometer, was used to record emission decays on the Infinium oscilloscope (Hewlett-Packard) coupled to the output of the PMT. A third harmonic (355 nm) from a nanosecond pulsed Nd:YAG laser (Lotis TII, Belarus), operating at 20 Hz, was used as the excitation source.

The xenografted mouse models were generated by subcutaneously injecting Panc-1 cells at a concentration of 2-3×10^6 cells/mouse in the scapular region of 5-6 week old female athymic nude mice (Hsd:Athymic Nude-*Foxn1*^{nu}) using a 1mL Monoject tuberculin syringe. Tumor growth was monitored every 24-48 hrs until a tumor size of approximately 5 mm in diameter was observed. The tumored mice was injected with the 200 μL of the nanoparticle formulation (30 μg/mL) in water with 5% glucose and imaged at different time points starting 2 hrs to 96 hrs post injection to study the biodistribution of the nanoparticle formulation in tumor and other major organs.

RESULTS AND DISCUSSIONS

Dynamic light scattering (DLS) studies were carried out to determine the hydrodynamic diameter of the nanomicelles. The size of the polymeric micelles varies with the loading of the Pt(TPNP) with the polymer showing the dependence of size on the polymer to dye ratio. Depending upon the polymer to Pt(TPNP) ratio, the hydrodynamic size of the polymeric nanomicelles varied between ~130 nm to 170 nm (Table 1).

The dimension and morphology of the polymeric nanoparticle formulation were further characterized by transmission electron microscopy (TEM) using a JEOL model JEM-100CX microscope operating at an acceleration voltage of 80 kV. To visualize the phospholipid layer, the samples were negatively stained using 1% PTA (phosphotungstic acid) at pH 7. With this technique, the stained phospholipid micelles doped with Pt(TPNP) can be visualized as irregular shaped light disks with average diameter at around 100 nm that stand out against the stained dark background (Figure 2).

Photophysical characterization of Pt(TPNP) in $CHCl_3$ and DSPE-PEG/PC nanomicelles was performed using absorption and photoluminescence spectroscopy. Results of the photophysical characterization of Pt(TPNP) are shown in Figure 3. Absorption and emission spectra of Pt(TPNP) in organic solvent are similar enough to those reported for Pt(II)-tetraphenyltetrabenzoporphyrin, Pt(TPBP).[30] Pt(TPNP) has the first absorption maximum at 691 nm and the emission peak at 903 nm, against 611 nm and 765 nm in case of Pt(TPBP). This bathochromic shift originates from the extension of the π-system by replacing the benzannulated phenyl group of Pt(TPBP) with a benzannulated naphthyl group in Pt(TPNP). The emission from the Pt(TPNP) is phosphorescence facilitated by a heavy-metal atom (Pt) which increases the rate of the intersystem crossing between singlet and triplet states of the metalloporphyrins, thereby enhancing the rate of radiative decay from the triplet state.[30, 56, 57] Absorption and emission of the Pt(TPNP) in DSPE-PEG/PC nanomicelles are close to that of Pt(TPNP) in $CHCl_3$, except strong quenching of phosphorescence from Pt(TPNP) in DSPE-PEG/PC with increase in concentration (Figure 3B). This is apparently caused by the aggregation of the metalloporphyrin molecules within micelles which dominates at the high ratios of Pt(TPNP) to DSPE-PEG/PC and leads to triplet-triplet annihilation.[58] Manifestation of this aggregation can be also seen in absorption spectra,[59-61]

when due to lower extinction of aggregates in comparison with that of monomers, a twofold increase in concentration results only in ~ 30% of increase in absorption intensity (Figure 3A curves 3,4). However at lower ratios of Pt(TPNP) to DSPE-PEG/PC, phosphorescence of the metalloporphyrin in polymeric nanomicelles is at least as efficient as in organic solvent. As can be seen in Figure 3C, phosphorescence decays of Pt(TPNP) in $CHCl_3$ as well as in DSPE-PEG/PC cannot be fitted to a single exponential but can be characterized by the average decay time, 3.3-3.9 μs for Pt(TPNP) in DSPE-PEG/PC, and ~1.3 μs for Pt(TPNP) in $CHCl_3$. It should be noted that room temperature phosphorescence is highly sensitive to the environment. Longer phosphorescence lifetime of Pt(TPNP) when they are encapsulated within polymeric micelles, over that when they are dissolved in an organic solution, can be explained, in particular, by a hindered access of quenchers, i.e. oxygen molecules. Phosphorescence quantum yield (φ_{ph}) was measured, using methanol solution of indocyanine green dye (fluorescence quantum yield of 0.12[62]) as a reference (see Supporting information), and was found to be 0.01. Taking into account that φ_{ph} of Pt(TPNP) in argon degassed toluene was reported to be 0.22,[35] one can suggest that the phosphorescence of Pt(TPNP) in micelles is strongly quenched by oxygen. However, we have found that purging of the Pt(TPNP)/DSPE-PEG/PC dispersion with nitrogen results in only ~25-30% increase in the phosphorescence intensity of the Pt(TPNP) (Figure 4D). This can be explained by the encapsulation of the Pt(TPNP) within polymeric micelles, which significantly hinders access by oxygen molecules, similarly to that reported for dendrimers with Pd/Pt porphyrin cores.[52, 63] Thus, factors other than the presence of oxygen are possibly playing major roles in the quenching of Pt(TPNP) phosphorescence within micelles. Probably this quenching is a result of intramolecular interactions (aggregation of the metalloporphyrin molecules) taking place within micelles, as indicated in Figures 3A and 3B.

We believe that, even if phosphorescence quantum yield of the investigated Pt(TPNP)/ DSPE-PEG/PC formulation is found to be not high, it will still be useful in optical imaging applications, considering the high molar extinction coefficient of the absorption band peaked at 691 nm, which is the spectral range where phosphorescence is observed and large spectral separation of the excitation and emission wavelengths. In addition, excitation/emission of the Pt(TPNP) is red-shifted in a comparison with previously reported NIR phosphorescent probes, thus allowing deeper tissue penetration and less background signal (scattering and autofluorescence) during imaging. While the absence of oxygen mediated strong phosphorescence quenching of the Pt(TPNP)/DSPE-PEG/PC nanomicelles impedes their use for imaging hypoxic tissues in vivo, it favors their use as nanoparticulate probes for optical imaging in vivo. All these results, along with excellent colloidal stablility of the Pt(TPNP)/DSPE-PEG/PC nanomicelles, prompted us to investigate their applicability in NIR phosphorescence optical imaging *in vivo*. Since the stability of nanomicelles is of importance for optical imaging, we have also tested a possible leakage of the entrapped Pt(TPNP) from DSPE-PEG/PC micelles. The release kinetics study has shown that the release of the Pt(TPNP) from micelles was insignificant, when Pt(TPNP)/DSPE-PEG/PC nanomicelles were incubated with 1% of the Tween-80 surfactant at 37°C (see Supporting information).

We have tested the cytotoxicity of the Pt(TPNP)/DSPE-PEG/PC nanomicelles by performing cell viability (MTS) assay[64] ,which was carried out with pancreatic cancer cell line Panc-1 (ATCC, CRL-1469), showing slight, dose-dependent toxicity of the nanomicelles over a period of 24hrs (see Supporting information). The nanoparticle formulation showed also no overt short-term toxicity in the injected mice after 96 hrs postinjection.

To verify the applicability the Pt(TPNP)/DSPE-PEG/PC nanomicelles for in vivo optical imaging and their possible tumor targeting ability, we injected them intravenously (tail vein) in nude mice bearing subcutaneous pancreatic tumor xenografts. *In vivo* PL imaging was accomplished using the Maestro GNIR FLEX fluorescence imaging system (CRi) (for details, see Supporting information). The phosphorescent dye formulation was excited using a "Deep red" excitation filter (CRi), transmitting light from the source (Xe lamp) in the range of 650-700 nm. An NIR emission filter (800 LP) in front of the imaging CCD camera was used to cut off the excitation light. Figure 4 presents results of the *in vivo* imaging. The whole-body images of the tumored nude mouse injected with nanomicelles were taken at various time points post-injection, and spectrally unmixed using the Maestro imaging software. The high contrast images clearly demonstrate the feasibility to spectrally distinguish and image the phosphorescence from Pt(TPNP) (shown as red). Figure 4B shows spectral profiles used to unmix the images shown in Figure 4A; spectral signatures from backgrounds 1 and 2 were sampled from the imaging stage and pre-injected mouse, respectively; an intense NIR emission spectrum peaked at around 900 nm was acquired from the vial with the Pt(TPNP)/DSPE-PEG/PC nanomicelles. As can be clearly seen in the Figure 4A, there is an intense phosphorescence from the tumor at 24 and 96 hrs post injection, while the 2 hrs post-injection image shows only a bright signal at the injection site (tail). Some emission from nanomicelles still can be seen in the lower abdominal region and in the liver, when mouse was imaged from the dorsal side (see Supporting information). It is quite evident that with a longer time period (24-96 hrs post injection) the accumulation of the Pt(TPNP)/DSPE-PEG/PC nanomicelles in the tumor takes place, although considerable amount of the phosphorescence can be observed in the liver as well. This can be attributed to the prolonged circulation time of the Pt(TPNP)/DSPE-PEG/PC nanomicelles, thus facilitating their passive tumor uptake via the EPR effect[22, 23] However, a release of the Pt(TPNP) from nanomicelles in vivo can also contribute to tumor targeting,[65] thus exploiting possible specificity of the porphyrin based molecules towards cancer cells[66]. Thus, tumor targeting ability of the Pt(TPNP)/DSPE-PEG/PC nanomicellar formulation can be caused by both EPR effect for the polymeric micelles and possible inherent tumor-avidity of Pt(TPNP), resulting in efficient labeling of the xenografted tumors in vivo. Further work needs to be done to clarify the mechanism of tumor targeting for the Pt(TPNP)/DSPE-PEG/PC nanomicelles.

Figure 4C visualizes a biodistribution of the nanomicelles in major organs. To carry out the studies, organs were resected after 96 hrs and imaged immediately, keeping the same parameters as for whole body in vivo imaging. The biodistribution results confirmed the accumulation of the polymeric nanomicelles mainly in the tumor and liver. It is interesting to note that phosphorescence from the liver bleeds through the back of the mouse (Figure 4A, 24, 96 hrs), illustrating better tissue penetration for the NIR light. The amount of the phosphorescence observed in other organs was insignificant.

Nanoparticles of different types are known to be efficiently captured by the liver,[67] but the relative amount of phosphorescence from the Pt(TPNP)/DSPE-PEG/PC nanomicelles which is seen in the tumor is quite remarkable. The phosphorescence intensity from the tumor looks even higher than that from the liver, thus implying a high efficiency of passive tumor targeting in our system, which is not observed in previous reports of passive tumor targeting employing other formulations of the DSPE-PEG nanomicelles and other PEG-grafted formulations.[68] Recently, Park et al[12] reported preparation and in vivo application of the PEG-phospholipid nanomicelles, co-doped with NIR emitting quantum dots, magnetic nanoparticles and anticancer drug for bimodal (optical and MRI) imaging and drug delivery and showed a moderate degree of tumor accumulation, which was significantly lower as compared to the liver accumulation. We believe that tumor specificity of the Pt(TPNP)/DSPE-PEG/PC nanomicelles can be even further improved by modifying the composition to

optimize their size distribution and/or surface properties, as well as incorporating biorecognition molecules on their surface for target specific delivery.[19-21, 69]

Following this, we have investigated whether it is possible to diagnose even smaller, visually undetectable subcutaneous tumors in mice using this phosphorescent nanomicellar formulation. With this purpose, we have intravenously injected the Pt(TPNP)/DSPE-PEG/PC nanomicelles in nude mice only one week following cancer cell inoculation. Visually undetectable small tumors demonstrated intense phosphorescence 24 hrs post injection of phosphorescent nanomicelles (Figure 5), thus demonstrating the ability of Pt(TPNP)/DSPE-PEG/PC formulation to detect tumors at very early stages of their development. In order to verify whether a local damage of the vasculature as a result of the injection of cancer cells is not a factor promoting accumulation of the phosphorescent micelles, a control experiment was performed. Here, non-tumored mouse was subcutaneously injected with saline, and subsequently injected in tail vein with Pt(TPNP)/DSPE-PEG/PC nanomicelles and imaged 24 hrs later. No localization of the Pt(TPNP)/DSPE-PEG/PC nanomicelles at the injected site was observed, thus suggesting the specificity of the formulation towards the tumor tissue (see Supporting information).

CONCLUSIONS

In conclusion, these nanosized probes for detection of cancer in a non-invasive manner can have significant clinical implications on cancer diagnostics and therapeutics. Based on all the preliminary results, it can be concluded that the phosphorescent polymeric nanomicellar formulation provides a powerful tool for *in vivo* optical imaging and carries a great promise as an efficient optical imaging probe aimed at the detection and imaging of tumors. Detailed studies with the micellar formulation are underway, including histo-pathological studies and studies using more advanced tumor models, including mice bearing orthotopically implanted spontaneously metastasizing pancreatic tumors.

Supplementary Material

Refer to Web version on PubMed Central for supplementary material.

Acknowledgments

This work was supported by grants form the National Institute of Health (R01CA119397 and RO1CA104492) and the John R. Oishei Foundation. We also thank Lisa A. Vathy for her technical support.

REFERENCES

1. Michaelis J, Hettich C, Mlynek J, Sandoghdar V. Nat. Med. 2000; 405:586.
2. Prasad, PN. Introduction to Biophotonics. Wiley-Interscience; New York: 2004.
3. Weissleder R. Nat. Biotechnol. 2001; 19:316. [PubMed: 11283581]
4. Sevick-Muraca EM, Houston JP, Gurfinkel M. Curr. Opin. Chem. Biol. 2002; 6:642. [PubMed: 12413549]
5. Kim S, Lim YT, Soltesz EG, De Grand AM, Lee J, Nakayama A, Parker JA, Mihaljevic T, Laurence RG, Dor DM, Cohn LH, Bawendi MG, Frangioni JV. Nat. Biotechnol. 2004; 22:93. [PubMed: 14661026]
6. Nyk M, Kumar R, Ohulchanskyy TY, Bergey EJ, Prasad PN. Nano Lett. 2008; 8:3834. [PubMed: 18928324]
7. Deissler V, Ruger R, Frank W, Fahr A, Kaiser WA, Hilger I. Small. 2008; 4:1240. [PubMed: 18666163]
8. Ghoroghchian PP, Frail PR, Susumu K, Blessington D, Brannan AK, Bates FS, Chance B, Hammer DA, Therien MJ. Proc. Natl. Acad. Sci. U.S.A. 2005; 102:2922. [PubMed: 15708979]

9. Altinoglu EI, Russin TJ, Kaiser JM, Barth BM, Eklund PC, Kester M, Adair JH. ACS Nano. 2008; 2:2075. [PubMed: 19206454]
10. Josephson L, Kircher MF, Mahmood U, Tang Y, Weissleder R. Bioconjugate Chem. 2002; 13:554.
11. He X, Nie H, Wang K, Tan W, Wu X, Zhang P. Anal. Chem. 2008; 80:9597. [PubMed: 19007246]
12. Park JH, von Maltzahn G, Ruoslahti E, Bhatia SN, Sailor MJ. Angew. Chem. Int. Ed. 2008; 47:7284.
13. Haacke, EMB.; R.W.; Thompson, ML.; Venkatesan, R. Magnetic Resonance Imaging: Physical Principles and Sequence Design. John Wiley; 1999.
14. Nahrendorf M, Zhang HW, Hembrador S, Panizzi P, Sosnovik DE, Aikawa E, Libby P, Swirski FK, Weissleder R. Circulation. 2008; 117:379. [PubMed: 18158358]
15. Shokeen M, Fettig NM, Rossin R. Q. J. Nucl. Med. Mol. Imaging. 2008; 52:267. [PubMed: 18475250]
16. Jain TK, Roy I, De TK, Maitra A. J. Am. Chem. Soc. 1998; 120:11092.
17. Esmaeili F, Ghahremani MH, Esmaeili B, Khoshayand MR, Atyabi F, Dinarvand R. Int. J. Pharm. 2008; 349:249. [PubMed: 17875373]
18. Esmaeili F, Ghahremani MH, Ostad SN, Atyabi F, Seyedabadi M, Malekshahi MR, Amini M, Dinarvand R. J. Drug Targeting. 2008; 16:415.
19. Leuschner C, Kumar CSSR, Hansel W, Soboyejo W, Zhou JK, Hormes J. Breast Cancer Res. and Treatment. 2006; 99:163.
20. Byrne JD, Betancourt T, Brannon-Peppas L. Adv. Drug Del. Rev. 2008; 60:1615.
21. Kirpotin DB, Drummond DC, Shao Y, Shalaby MR, Hong KL, Nielsen UB, Marks JD, Benz CC, Park JW. Cancer Res. 2006; 66:6732. [PubMed: 16818648]
22. Lukyanov AN, Gao ZG, Mazzola L, Torchilin VP. Pharm. Res. 2002; 19:1424. [PubMed: 12425458]
23. Maeda H, Wu J, Sawa T, Matsumura Y, Hori K. J. Controlled Release. 2000; 65:271.
24. Torchilin VP. Pharm. Res. 2007; 24:1. [PubMed: 17109211]
25. Roby A, Erdogan S, Torchilin VP. Cancer Biol. Therapy. 2007; 6:1136.
26. Skidan I, Dholakia P, Torchilin V. J. Drug Targeting. 2008; 16:486.
27. Baldo MA, O'Brien DF, You Y, Shoustikov A, Sibley S, Thompson ME, Forrest SR. Nature. 1998; 395:151.
28. Brooks J, Babayan Y, Lamansky S, Djurovich PI, Tsyba I, Bau R, Thompson ME. Inorg. Chem. 2002; 41:3055. [PubMed: 12054983]
29. Chou PT, Chi Y. Chem.-Eur. J. 2007; 13:380. [PubMed: 17146830]
30. Borek C, Hanson K, Djurovich PI, Thompson ME, Aznavour K, Bau R, Sun YR, Forrest SR, Brooks J, Michalski L, Brown J. Angew. Chem. Int. Ed. 2007; 46:1109.
31. Sun Y, Borek C, Hanson K, Djurovich PI, Thompson ME, Brooks J, Brown JJ, Forrest SR. Appl. Phys. Lett. 2007; 90:263503.
32. Sun YR, Giebink NC, Kanno H, Ma BW, Thompson ME, Forrest SR. Nature. 2006; 440:908. [PubMed: 16612378]
33. Baldo MA, Lamansky S, Burrows PE, Thompson ME, Forrest SR. Appl. Phys. Lett. 1999; 75:4.
34. Yersin H. Transition Metal and Rare Earth Compounds III. 2004; 241:1.
35. Sommer JR, Farley RT, Graham KR, Yang Y, Reynolds JR, Xue J, Schanze KS. ACS *Appl. Mater. & Interf.*. 2009; 1:274.
36. deHaas RR, vanGijlswijk RPM, vanderTol EB, Zijlmans HJMAA, BakkerSchut T, Bonnet J, Verwoerd NP, Tanke HJ. J. Histochem. Cytochem. 1997; 45:1279. [PubMed: 9283615]
37. Botchway SW, Charnley M, Haycock JW, Parker AW, Rochester DL, Weinstein JA, Williams JAG. Proc. Natl. Acad. Sci. U.S.A. 2008; 105:16071. [PubMed: 18852476]
38. de Haas RR, van Gijlswijk RPM, van der Tol EB, Veuskens J, van Gijssel HE, Tijdens RB, Bonnet J, Verwoerd NP, Tanke HJ. J. Histochem. Cytochem. 1999; 47:183. [PubMed: 9889254]
39. Apreleva SV, Wilson DE, Vinogradov SA. Optics Lett. 2006; 31:1082.
40. Apreleva SV, Wilson DF, Vinogradov SA. Appl. Optics. 2006; 45:8547.

41. Yu MX, Zhao Q, Shi LX, Li FY, Zhou ZG, Yang H, Yia T, Huang CH. Chem. Comm. 2008; 18:2115. [PubMed: 18438486]
42. Amoroso AJ, Arthur RJ, Coogan MP, Court JB, Fernandez-Moreira V, Hayes AJ, Lloyd D, Millet C, Pope SJA. New J. Chem. 2008; 32:1097.
43. Amoroso AJ, Coogan MP, Dunne JE, Fernandez-Moreira V, Hess JB, Hayes AJ, Lloyd D, Millet C, Pope SJA, Williams C. Chem. Comm. 2007; 29:3066. [PubMed: 17639143]
44. Lo KKW, Louie MW, Sze KS, Lau JSY. Inorg. Chem. 2008; 47:602. [PubMed: 18088115]
45. Lo KKW, Lee TKM, Lau JSY, Poon WL, Cheng SH. Inorg. Chem. 2008; 47:200. [PubMed: 18067284]
46. Pfister A, Zhang G, Zareno J, Horwitz AF, Fraser CL. ACS Nano. 2008; 2:1252. [PubMed: 19081748]
47. Kurner JM, Klimant I, Krause C, Preu H, Kunz W, Wolfbeis OS. Bioconjugate Chem. 2001; 12:883.
48. Kurner JM, Klimant I, Krause C, Pringsheim E, Wolfbeis OS. Anal. Biochem. 2001; 297:32. [PubMed: 11567525]
49. Song X, Huang L, Wu B. Anal. Chem. 2008; 80:5501. [PubMed: 18510340]
50. Rumsey WL, Vanderkooi JM, Wilson DF. Science. 1988; 241:1649. [PubMed: 3420417]
51. Wilson DF, Rumsey WL, Green TJ, Vanderkooi JM. J. Biol. Chem. 1988; 263:2712. [PubMed: 2830260]
52. Brinas RP, Troxler T, Hochstrasser RM, Vinogradov SA. J. Am. Chem. Soc. 2005; 127:11851. [PubMed: 16104764]
53. Perez DM, Borek C, Forrest SR, Thompson ME. J. Am. Chem. Soc. submitted.
54. Cinteza LO, Ohulchanskyy TY, Sahoo Y, Bergey EJ, Pandey RK, Prasad PN. Mol. Pharm. 2006; 3:415. [PubMed: 16889435]
55. Zheng Q, Ohulchanskyy TY, Sahoo Y, Prasad PN. J. Phys. Chem. C. 2007; 111:16846.
56. Chandra AK, Turro NJ, Lyons AL, Stone P. J. Am. Chem. Soc. 1978; 100:4964.
57. Papkovsky DB. Sens. Actuators B. 1995; 29(1-3):213–218.
58. Turro NJ, Aikawa M. J. Am. Chem. Soc. 1980; 102:4866.
59. Pugh D, Giles CH, Duff DG. Trans. Faraday Soc. 1971; 67:563.
60. Gandini SCM, Yushmanov VE, Borissevitch IE, Tabak M. Langmuir. 1999; 15:6233.
61. Li XY, He X, Ng ACH, Wu C, Ng DKP. Macromolecules. 2000; 33:2119.
62. Philip R, Penzkofer A, Baumler W, Szeimies RM, Abels C. J. Photochem. Photobiol. A. 1996; 96:137.
63. Rozhkov V, Wilson D, Vinogradov S. Macromolecules. 2002; 35:1991.
64. Cory AH, Owen TC, Barltrop JA, Cory JG. Cancer Comm. 1991; 3:207.
65. Chen HT, Kim SW, Li L, Wang SY, Park K, Cheng JX. Proc. Natl. Acad. Sci.U.S.A. 2008; 105:6596. [PubMed: 18445654]
66. Song R, Kim YS, Sohn YS. J. Inorg. Biochem. 2002; 89:83. [PubMed: 11931967]
67. Brigger I, Dubernet C, Couvreur P. Adv. Drug Delivery Rev. 2002; 54:631.
68. Torchilin VP. Eur. J. Pharm. Biopharm. 2009; 71:431. [PubMed: 18977297]
69. Torchilin V. Expert Opin. Drug Delivery. 2008; 5:1003.

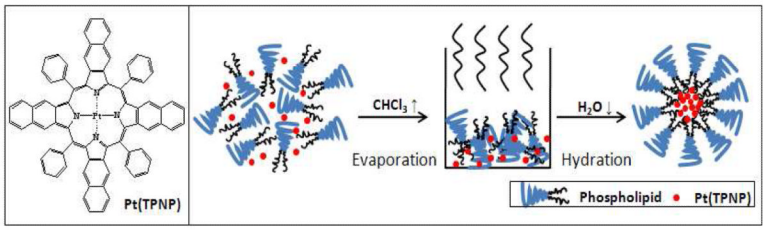

Figure 1.
Structure of the Pt(TPNP) and the scheme showing the procedure used to prepare polymeric nanomicelles encapsulating the Pt(TPNP) within PEG-modified phopholipid micelle.

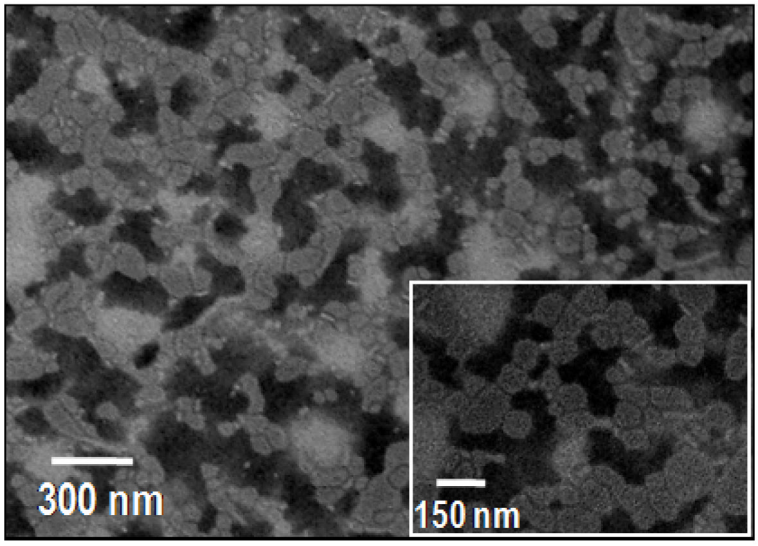

Figure 2.
Representative TEM images of the Pt(TPNP)/DSPE-PEG/PC nanomicelles.

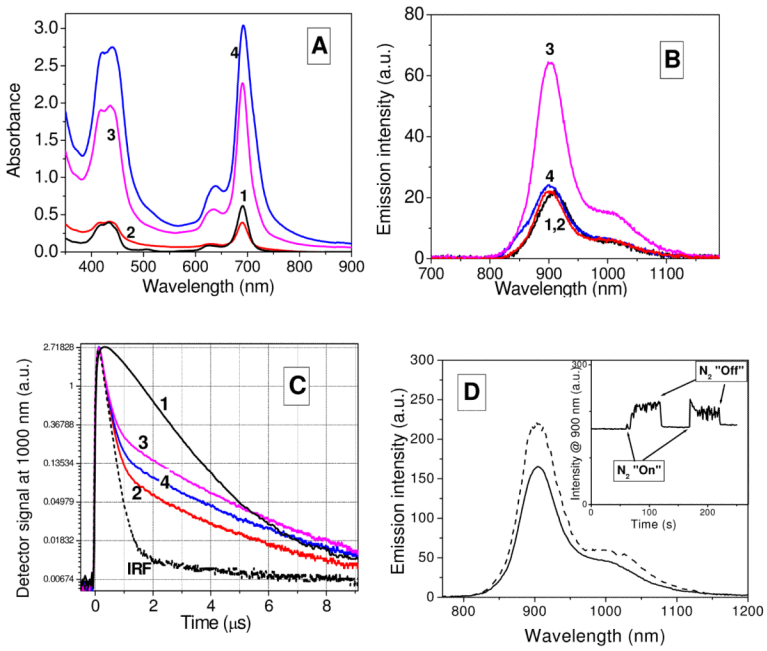

Figure 3.

Absorption (**A**), emission (**B**) spectra and emission decays (**C**) from Pt(TPNP) in $CHCl_3$ (1) and DSPE-PEG/PC nanomicelles (2-4) at room temperature. Concentrations of Pt(TPNP): 2.5 μM (1, 2), 12.5 μM (3), 25 μM (4). **D**. Pt(TPNP)/DSPE-PEG/PC phosphorescence spectra in presence of oxygen (solid line) and under nitrogen purging (dashed line). Inset shows change in the phosphorescence intensity at 900 nm with turning on/off N_2 bubbling.

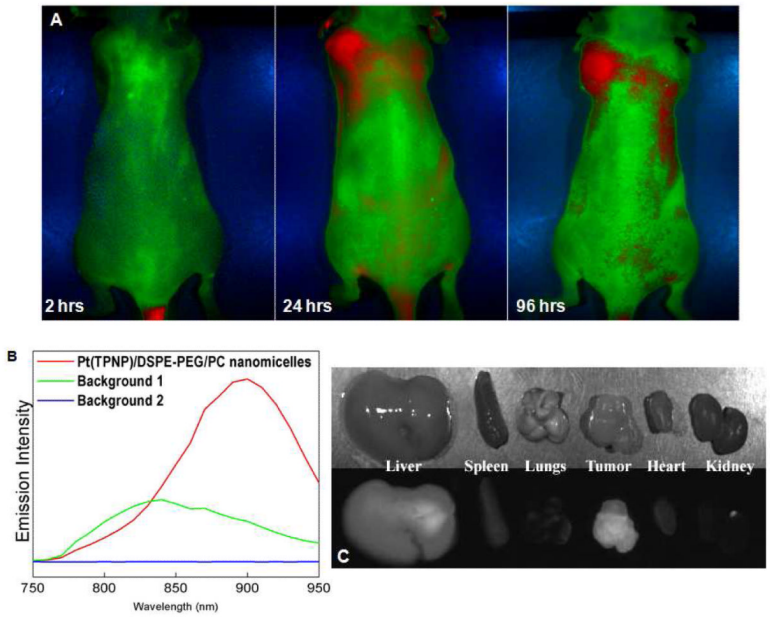

Figure 4.

A. PL images of the tumored nude mouse at various time points (2, 24, 96 hrs) post-injection with the nanomicelles. B. Spectral profiles used to unmix images shown in the panel A. C – Bright field and PL images of the major organs resected from mouse 96 hrs post-injection.

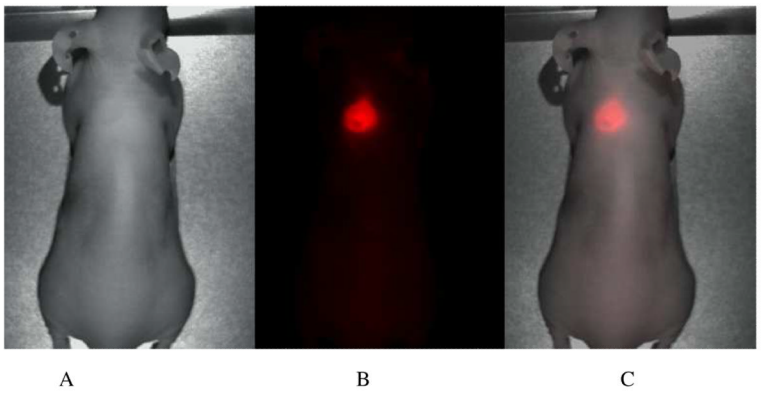

Figure 5.
Bright field (A), phosphorescence (B) and combined (C) images of the nude mouse xenografted with a subcutaneous Panc 1 tumor in its early phase of growth. (1 week after tumor cells injection). Images were taken 24 hrs after iv injection of the Pt(TPNP)/DSPE-PEG/PC nanomicelles.

Table 1

Average hydrodynamic size of the polymeric nanoparticle formulation containing different concentration of the Pt(TPNP)

Polymer/Pt(TPNP) (w/w)	1/0.006	1/0.003	1/0.0006
Conc of Pt(TPNP)	25μM	12.5μM	2.5 μM
Hydrodynamic diameter (nm)	172.6 ± 1.1	153.9 ± 1.5	132.8 ± 1.8
Polydispersity	0.212	0.118	0.209